Open Access

*Chemistry*OPEN

Full Papers

Oxo-Hydroxoferrate $K_{2-x}Fe_4O_{7-x}(OH)_x$: Hydroflux Synthesis, Chemical and Thermal Instability, Crystal and Magnetic Structures

Ralf Albrecht,[a] Jens Hunger,[a] Theresa Block,[b] Rainer Pöttgen,[b] Anatoliy Senyshyn,[c] Thomas Doert,*[a] and Michael Ruck*[a, d]

The reaction of $Fe(NO_3)_3 \cdot 9\,H_2O$ with KOH under hydroflux conditions at about 200 °C produces red crystals of $K_{2-x}Fe_4O_{7-x}(OH)_x$ in a quantitative yield. In the crystal structure, edge-sharing $[FeO_6]$ octahedra form $_\infty^2[Fe_2O_6]$ honeycomb nets. Pillars consisting of pairs of vertex-sharing $[FeO_4]$ tetrahedra link the honeycomb layers and form columnar halls in which the potassium ions are located. The trigonal ($P\bar{3}1m$) and the hexagonal ($P6_3/mcm$) polytypes of $K_{2-x}Fe_4O_{7-x}(OH)_x$ show oriented intergrowth. The sub-stoichiometric potassium content ($x \approx 0.3$) is compensated by hydroxide ions. $K_{2-x}Fe_4O_{7-x}(OH)_x$ is an antiferromagnet above 2 K and its magnetic structure was determined by neutron powder diffraction. Under ambient conditions, $K_{2-x}Fe_4O_{7-x}(OH)_x$ hydrolyzes and $K_2CO_3 \cdot H_2O$ forms gradually on the surface of the $K_{2-x}Fe_4O_{7-x}(OH)_x$ crystals. Upon annealing at air at about 500 °C, the potassium atoms in the columnar halls start to order into a superstructure. The thermal decomposition of $K_{2-x}Fe_4O_{7-x}(OH)_x$ proceeds via a topotactic transformation into $K_{1+x}Fe_{11}O_{17}$, adopting the rhombohedral β″ or the hexagonal β-aluminate-type structure, before γ-Fe_2O_3 is formed above 950 °C, which then converts into thermodynamically stable α-Fe_2O_3.

1. Introduction

Iron oxides and oxoferrates are used in manifold ways, e.g. hexaferrites like $BaFe_{12}O_{19}$ as magnetic storage materials,[1] $BaFeO_{2.5}$ as ion conductor in oxidic high-temperature fuel cells,[2] or hematite Fe_2O_3 in solar cell technology.[3,4] Beside these examples, there is a variety of other applications for oxidic iron compounds. The high usability of iron results from its unique combination of properties, such as strong magnetism in almost all of its oxidation states,[5] the adoptable coordination,[6] and last but not least, the overwhelming availability on earth.[7] Iron oxides were studied extensively over many decades, however, there are still new discoveries in the field of alkali and alkaline earth metal ferrates, such as the potassium ferrate $K_2Fe_4O_7$, which is a superionic conductor, e. g.[8–10]

In recent decades, many potassium ferrates have been synthesized, all of them by applying synthesis temperatures above 400 °C. The hydroflux method,[11] which we used for the synthesis of $K_{2-x}Fe_4O_{7-x}(OH)_x$ is a new approach to access (metastable) alkali metal ferrates. The properties of a hydroflux medium are similar to a hydroxide flux: strongly basic character, high solubility for oxidic compounds, and reasonably high stability against oxidation. Adding comparatively small amounts of water successively lowers the melting point of the alkali flux (neat KOH: 360 °C, $KOH \cdot H_2O$: 143 °C) so that even syntheses at room temperature are possible.

Besides the hydroflux synthesis, this paper reports a detailed study of $K_{2-x}Fe_4O_{7-x}(OH)_x$, including some hitherto unknown features, such as its intrinsic non-stoichiometry and iron mixed valence, polytypic structures, its chemical and thermal decomposition, its magnetic properties and its electrical resistance.

2. Results and Discussion

2.1. Synthesis

Red crystals of $K_{2-x}Fe_4O_{7-x}(OH)_x$ (yield > 99 %) were obtained by reacting iron(III) nitrate nonahydrate with a mixture of potassium hydroxide and water (molar ratio $n(H_2O):n(KOH) = 1.2$) in a PTFE-lined stainless steel autoclave. Due to the highly corrosive medium, the required constant base concentration and the moderate reaction temperatures, the use of a PTFE-lined autoclave was deemed prudent, although almost no pressure was generated during the reaction.[12] A screening of the

[a] R. Albrecht, Dr. J. Hunger, Prof. Dr. T. Doert, Prof. Dr. M. Ruck
    Faculty of Chemistry and Food Chemistry,
    TU Dresden, 01062 Dresden (Germany)
    E-mail: thomas.doert@tu-dresden.de
         michael.ruck@tu-dresden.de
    Homepage: http://chm.tu-dresden.de/ac2/
[b] T. Block, Prof. Dr. R. Pöttgen
    Institut für Anorganische und Analytische Chemie,
    WWU Münster, Corrensstraße 30, 48149 Münster (Germany)
[c] A. Senyshyn
    Department of Physics, TU München,
    Lichtenbergstraße 1, 85748 Garching (Germany)
[d] Prof. Dr. M. Ruck
    Max-Planck Institute for Chemical Physics of Solids,
    Nöthnitzer Straße 40, 01187 Dresden (Germany)

synthesis parameters showed that the reaction is complete even at 100 °C, but yields in small crystallites with sizes below 50 μm. The average particle size increases with reaction temperature and crystallites of about 150 μm were obtained between 200 and 230 °C within 10 h. The formation of the product is complete after a few hours. A similar observation has been made by geoscientists in 2014.[13] They described the solvation of chromium ore by highly concentrated potassium hydroxide solution (molar ratio $n(H_2O) : n(KOH) = 1.34$), analyzing the progress of the reaction by the crystallization of $K_{2-x}Fe_4O_{7-x}$ $(OH)_x$, which was erroneously stated as "KFe_3O_5" based on EDX analyses. According to X-ray powder diffraction (PXRD) a prolongation of the reaction time beyond 50 h results in a large amount of α-Fe_2O_3 as by-product, reaction times exceeding 100 h result in phase pure hematite only, pointing towards a slow decomposition of $K_{2-x}Fe_4O_{7-x}(OH)_x$. A change of the base concentration also results in side products, like α-Fe_2O_3.

2.2. Crystal Structure, Polytypism, and Non-stoichiometry

X-ray diffraction on a single-crystal at 100(1) K revealed the composition $K_{2-x}Fe_4O_7$ with $x = 0.31(1)$ and a trigonal structure in the space group $P\bar{3}1m$ (no. 162) (Table S1, Supporting Information) with lattice parameters $a = 517.51(1)$ pm and $c = 692.27(2)$ pm (at $T = 298$ K: $a = 518.35(2)$ pm, $c = 693.04(3)$ pm). The iron atoms are located in octahedral (Fe1) as well as in tetrahedral oxygen environment (Fe2) with equal multiplicities (Figure 1). The [FeO₆] octahedra are linked via common edges
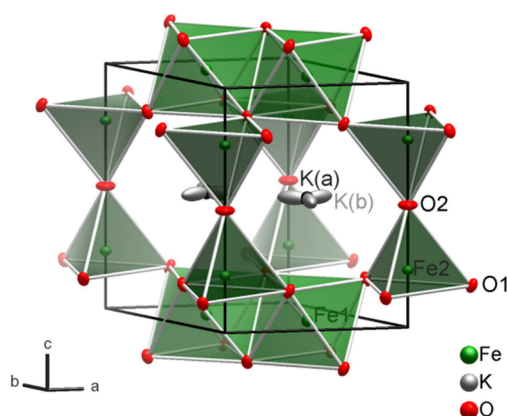

Figure 1. Crystal structure of $K_{2-x}Fe_4O_{7-x}(OH)_x$ ($P\bar{3}1m$ polytype). Ellipsoids enclose 90 % of the probability density of the atoms at 100 K. For details on the occupation of the potassium positions, see text.

to form a hexagonal honeycomb net $_\infty^2[Fe_2O_6]$ (Figure 2). The [FeO₄] tetrahedra cap both sides of the hexagonal voids of the honeycomb net by sharing vertices with three octahedra. [FeO₄] tetrahedra of neighboring layers share their apical vertices, forming pillars between the honeycomb layers. Overall, a three-dimensional oxoferrate framework results that encloses cavities between the pillars, in which the potassium atoms reside. Every potassium atom is surrounded by nine oxygen atoms in the
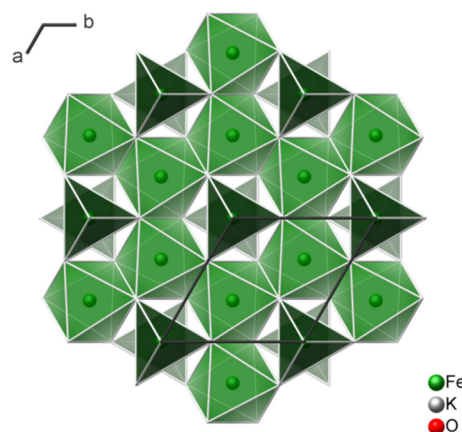

Figure 2. Oxoferrate layer in the crystal structure of $K_{2-x}Fe_4O_{7-x}(OH)_x$ ($P\bar{3}1m$ polytype). The tetrahedra cap the hexagonal voids in the honeycomb formed by octahedra. The potassium cations (not shown) reside above and below the iron atoms of the octahedra.

shape of a tri-capped trigonal antiprism. The [KO₉] polyhedra share rectangular faces with an area of about $12 \cdot 10^4$ pm². This structural motif had been reported for $BaFe_4O_7$ and $K_{0.22}Ba_{0.89}Fe_4O_7$[14] as well as for the high pressure phases $A_2Mg_2Si_2O_7$ ($A = Na$, K).[15,16]

For many $K_{2-x}Fe_4O_{7-x}(OH)_x$ crystals we found diffuse scattering contributions or weak additional reflections in the diffraction pattern and conspicuous residuals in the difference Fourier maps ($F_o - F_c$) originating from an alternative stacking of tetrahedra. While in the dominating trigonal sequence described above, the vertex sharing tetrahedra are staggered, an eclipsed conformation gives rise to a second polytype. In the case of strict periodicity this leads to a unit cell with doubled c-axis and the space group $P6_3/mcm$ (Figure 3). Stacking faults or oriented intergrowth of larger domains of the $P\bar{3}1m$ and $P6_3/mcm$ polytypes are common and can be understood by order-disorder (OD) theory.[14–20] OD theory uses the theory of group-

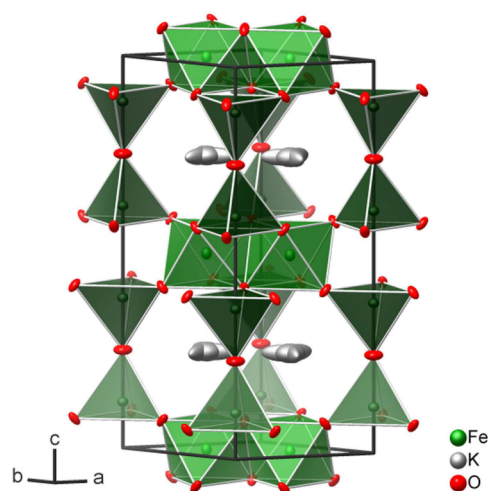

Figure 3. Crystal structure of $K_{2-x}Fe_4O_{7-x}(OH)_x$ ($P6_3/mcm$ polytype). Ellipsoids enclose 90 % of the probability density of the atoms at 100 K. For details on the occupation of the potassium positions see text.

oids to pairs of crystallochemically equivalent layers to describe stacking disorder. Such pairs are related by symmetry operations, which do not apply for the whole structure.

The structure refinement on $K_{2-x}Fe_4O_{7-x}(OH)_x$ revealed two symmetrically inequivalent potassium positions, which are both partially occupied: K(a) (Wyckoff position 2d, site symmetry 3.2) is occupied to approximately 38 %. The three nearby K(b) positions (6j, ..2) are occupied to about 15 % each (Figure 1). The potassium deficiency was confirmed by EDX analyses on single crystals and by ICP-OES analyses on bulk samples. Structure refinements on different crystals resulted in rather similar compositions ($0.3 \leq x \leq 0.35$). Neither X-ray nor neutron data (see below) provide evidence for oxygen deficiencies or hydrogen atoms; difference Fourier maps are featureless within the limits of the method (Figure S1, Supporting Information).

The voids on the K(a) site obviously cause the displacement of neighboring potassium atoms on the position K(b). Moreover, the oxygen atom O2 (1b, $\bar{3}.m$), which is in the center of the pillar and at the same height in z as the potassium atoms, shows a disk-shaped displacement ellipsoid, which is not unusual for bridging oxygen atoms of corner-sharing tetrahedral. However, a certain response to the potassium disorder seems also likely.

The potassium off-stoichiometry was not reported for materials in references[8–10] although obtained under similar reaction conditions and described with analogous structural data.

An (hypothetical) ordered superstructure model of a potassium-deficient iron ferrate can be constructed for $x = 0.5$, i.e., $K_{1.5}Fe_4O_7H_{0.5}$ (Figure 4). In this model, one fourth of the
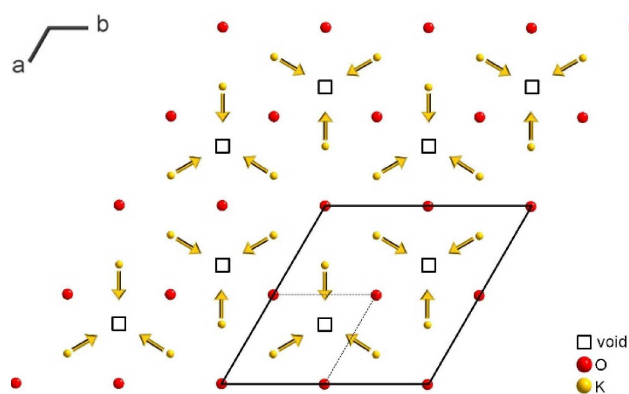

Figure 4. Superstructure model with $a' = 2a$ and $b' = 2b$ including the ordering of voids and shifting of neighboring atoms in the layer at $z = 0.5$ for hypothetical $K_{1.5}Fe_4O_7H_{0.5}$. The dotted line indicates the unit cell of $K_{2-x}Fe_4O_{7-x}(OH)_x$.

potassium positions are vacant (i.e. no K(a)) and these voids are surrounded by fully occupied potassium positions K(b) that are shifted towards the voids. This arrangement comprises a doubling of the lattice parameters a and b, but maintains the space group type of $P\bar{3}1m$. However, all attempts to obtain an ordered structure of the composition $K_{1.5}Fe_4O_7H_{0.5}$ failed so far.

2.3. Charge Balancing, Valence States and Hydrogen Content

Assuming K^+, Fe^{3+} and O^{2-}, the potassium sub-stoichiometry of $x \approx 0.3$ results in the non-charge-balanced formula "$K_2Fe_4O_7$". Charge balancing could be realized by either unrecognized lithium or sodium admixtures (potential impurities in KOH), oxygen vacancies, hydroxide groups, or a partial oxidation of iron(III) to iron(IV).

Sodium and lithium impurities could be excluded by ICP-OES measurements and EDX analyses (for sodium) within the limits of the methods (Figure S2, Table S2 and S3, Supporting Information). Sizeable oxygen vacancies were excluded by structure refinements on data from single-crystal X-ray diffraction and powder neutron diffraction (see below) and supported by EDX analyses on several crystals. Traceable amounts of hydrogen are expected to give a considerably large diffuse background in the neutron powder diagram due to the enormous incoherent scattering contribution of normal hydrogen. This is, however, not the case in our neutron data, Figures S3 and S4, Supporting Information.

The presence of hydrogen was also tested by solid-state ^{1}H-NMR spectroscopy and IR spectroscopy (tracing OH-vibrations). Static and dynamic (magic angle spinning) solid state ^{1}H-NMR spectra showed no signal in the whole spectral range from $-5 \leq \delta \leq 20$ ppm (Figure S5, Supporting Information). The IR spectrum of a $K_{2-x}Fe_4O_{7-x}(OH)_x$ sample stored under argon (Figure S6, Supporting Information) shows a tiny absorption band at 3570 cm^{-1}, which might be understood as a O—H valence vibration (ν_{OH}).[21] The fact that this signal is sharp and at wave numbers near to those of free OH ions (3556 cm^{-1}) should then indicate isolated OH groups and exclude hydrogen bonds.[22] Further bands are found at 783 cm^{-1}(strong, s), 534 cm^{-1} (very strong), 365 cm^{-1} (s) and 304 cm^{-1} (s). A $K_{2-x}Fe_4O_{7-x}(OH)_x$ sample stored in air showed additional weak vibrational bands at 1650 cm^{-1}, 1557 cm^{-1}, 1390 cm^{-1}. The H—O—H bending mode of water can be related to the weak band at 1650 cm^{-1} in the latter sample due to sample decomposition (see below). The vibration band at 1390 cm^{-1} could also be caused by segregated KOH or $K_2CO_3 \cdot H_2O$ at the surface of the potassium ferrate crystals (see below). The remaining bands in the IR spectrum of $K_{2-x}Fe_4O_{7-x}(OH)_x$ are probably caused by Fe—O valence vibrations. The bands at 534 cm^{-1} and at 365 cm^{-1} and 304 cm^{-1} can be assigned to [FeO$_6$] octahedra (T_{1u}) and [FeO$_4$] tetrahedra (C_{3v}), respectively, by comparison with the IR spectra of magnetite and hematite.[23,24] The band at 783 cm^{-1} could be caused by the short Fe—O bond of the bridging tetrahedra (Table S6, Supporting Information).

Mößbauer spectroscopy was applied to probe the oxidation state of iron. The spectrum recorded at $T = 6$ K (Figure 5) shows a magnetically split sextet, which confirms the magnetic order of $K_{2-x}Fe_4O_{7-x}(OH)_x$. The spectrum can be fitted adequately by assuming three different contributions (Table 1): one sextet with a contribution of 49(2) % of the total transmission integral and a typical isomer shift ($\delta = 0.37(1)$) for octahedrally coordinated iron(III) (Fe$_{oct}$), and two sextets with significantly smaller isomer shifts of $\delta = 0.18(1)$ and $\delta = 0.21(1)$ contributing to 41(2)
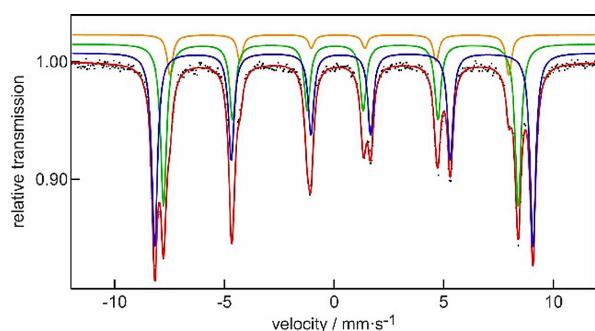
Figure 5. ^{57}Fe Mößbauer spectrum of $K_{2-x}Fe_4O_{7-x}(OH)_x$ at $T = 6$ K with the measured intensities (black dots) and the fittings of the sub-spectra (for details, see Table 1).

Table 1. Fitting parameters of ^{57}Fe Mößbauer spectroscopic measurements of $K_{2-x}Fe_4O_{7-x}(OH)_x$ at $T = 6$ K; $\delta =$ isomer shift, $\Delta E_Q =$ electric quadrupole shift, $\Gamma =$ experimental line width, $B_{hf} =$ hyperfine splitting. The color code for the sub-spectra of Figure 1 is indicated.

Valence state	δ [mm·s^{-1}]	ΔE_Q [mm·s^{-1}]	Γ [mm·s^{-1}]	B_{hf} [T]	Ratio [%]
Fe$^{III}_{oct.}$ (blue)	0.37(1)	0.14(1)	0.31(1)	53.50(1)	49(2)
Fe$^{III}_{tetr.}$ (green)	0.18(1)	0.26(1)	0.33(1)	50.16(1)	41(2)
Fe$^{III}_{tetr}$ (ocher)	0.21(1)	0.06(1)	0.31(1)	47.93(3)	10(2)

% and 10(2) %, respectively. The latter two can be understood as originating from tetrahedrally coordinated iron(III) (Fe$_{tet}$).[25] None of these isomer shifts is in the expected range for iron(IV) in octahedral or tetrahedral oxygen coordination.[25] Assuming a mixed-valent compound with iron(III) and iron(IV) on the same crystallographic site, one could also expect a signal with an intermediate iron(III)$_{tet}$/iron(IV)$_{tet}$ isomer shift at high temperatures. Lowering the temperature should resolve the valence fluctuations and lead to two distinct signals, which is, however, not observed.

Carrier gas hot extraction (CGHE) probes an oxygen content of 26.2(5) wt.-% and a hydrogen content of 0.14(1) wt.-%. The latter seems too high to stem from for a partial sample decomposition only. Estimating reasonable confidence intervals, the combined analytical data can be translated into a charge-balanced formula $K_{2-x}Fe_4O_{7-x}(OH)_x$ with $x = 0.3$. (Note: The CGHE derived hydrogen amount is even higher than expected for $x = 0.3$). On this basis $K_{2-x}Fe_4O_{7-x}(OH)_x$ can be called a potassium oxo-hydroxoferrate(III). Because no hydrogen position can be deduced from the diffraction data, the structure images are thus displayed without H atoms and the structure description and crystal-chemical discussion focusses on the metal-oxygen framework.

The sub-stoichiometric hydrogen amount and the assumed static and – at least at higher temperatures – dynamic disorder impede the location of hydrogen atoms from the diffraction experiments. Most astonishingly, the neutron data at $T = 4$ K do not show pronounced maxima and minima in the difference Fourier map (Figure S1). The absence of an ^{1}H-NMR signal may be explained by the magnetic order of the compound even at ambient temperatures. As Mößbauer spectroscopy data suggest

two Fe$_{tet}$ species with different electrical field gradients at $T = 6$ K and following simple space filling considerations, the OH groups should most likely be located at the bridging positions connecting two FeO$_4$-tetrahedra. Since one bridging hydroxide group influences two Fe$_{tet}$ atoms we would expect a ratio of about 70:30 for an ordered situation (observed 80:20).

Low temperature diffraction data reveals that the electron density distribution at this bridging position is non-rotational symmetric indicating a slight dislocation of the oxygen atoms. This would also lead to a non-linear Fe—O—Fe coordination of the bridging oxygen atom which can, however, not be modelled with the presently available data.

2.4. Magnetism and Electrical Conductivity

Measurements of the magnetization of $K_{2-x}Fe_4O_{7-x}(OH)_x$ prove the compound to be magnetically ordered even beyond room temperature (Figure 6 and S7, Supporting Information). The
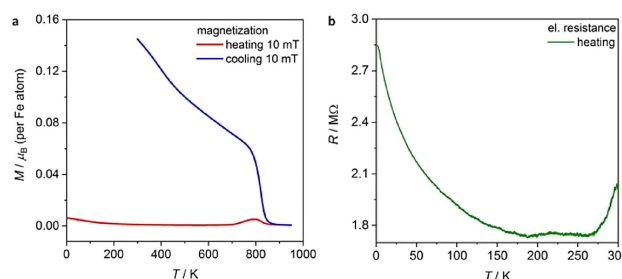

Figure 6. Temperature dependence of the magnetization (powder sample) in an external field of $\mu_0H = 10$ mT (a) and temperature dependence of the electrical resistance (single crystal) of a of $K_{2-x}Fe_4O_{7-x}(OH)_x$ (b).

apparent ordering temperature of approximately 567 °C (840 K) is probably that of ferrimagnetic $K_{1+x}Fe_{11}O_{17}$,[26,27] which starts to form above ca. 500 °C (see below). Since this transformation is irreversible, the cooling curve strongly deviates from the heating curve. The chemically and structurally related compounds BaFe$_4$O$_7$ and $K_{0.22}Ba_{0.89}Fe_4O_7$ were also reported to be antiferromagnets with exceptionally high magnetic ordering temperatures ($T_N > 850$ K).[14]

Rietveld refinement on neutron diffraction data of a powder sample of $K_{2-x}Fe_4O_{7-x}(OH)_x$ (Figure S3, S4 and Table S4, Supporting Information) confirms the antiferromagnetic order at 300 K and 4 K. The magnetic structure adopts the magnetic space group $P\bar{3}1c$ with lattice parameter c' doubled with respect to the nuclear structure. All moments are aligned parallel to [001]; no canting of the spins has been found in contrast to the magnetic structures of BaFe$_4$O$_7$ and $K_{0.22}Ba_{0.89}Fe_4O_7$.[14]

The spins on the iron atoms within each honeycomb layer of $K_{2-x}Fe_4O_{7-x}(OH)_x$ are ferromagnetically ordered, while the tetrahedrally coordinated iron atoms couple antiferromagnetically to all neighboring iron atoms (Figure 7), which also follows from the chosen symmetry of the magnetic structure on altering layers. All spins on iron atoms with the same z
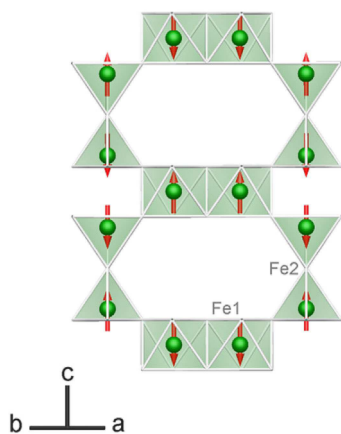
Figure 7. Magnetic structure of $K_{2-x}Fe_4O_{7-x}(OH)_x$. Red arrows indicate the spin orientation.

parameter have the same orientation. From the neutron data reduced magnetic moments of $\mu_{eff} = 3.97(4)$ μ_B for iron in the tetrahedra and $\mu_{eff} = 4.18(4)$ μ_B for iron in the octahedra at 4 K were calculated, significantly less than the spin only value of 5.92 μ_B for iron(III). A similar deviation had been observed for, e.g., $Sr_2FeO_3F^{[28]}$ or $Y_3Fe_5O_{12}$ and might be attributed to a covalent contribution to the Fe—O bonds.[29]

In accordance with the red color of the compound, the temperature dependent electrical resistivity indicates semiconducting behavior below 250 K (Figure 6). Remarkably, the electrical resistance increases with temperature above this temperature. This might be due to partial hydrolysis/decomposition and surface impurities like KOH and/or $K_2CO_3 \cdot H_2O$ (see below). A reasonably good ion conductivity was recently reported for $K_2Fe_4O_7$, which – based on the published structural data – seems to be the same compound without addressing the potassium non-stoichiometry.[9]

2.5. Chemical and Thermal Instability

After storing crystals of $K_{2-x}Fe_4O_{7-x}(OH)_x$ at ambient conditions for several weeks, white crystalline precipitates were found at their surfaces (Figure 8). EDX measurements on these precipitates indicate potassium, oxygen and carbon, so that we
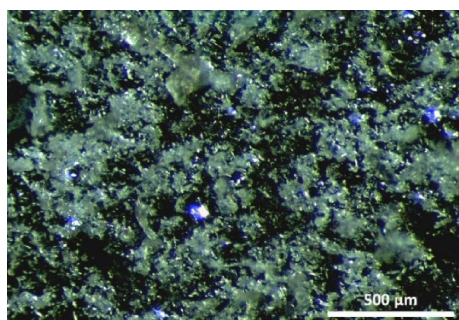
assume a potassium carbonate. Obviously, $K_{2-x}Fe_4O_{7-x}(OH)_x$ hydrolyzes under segregation of KOH which subsequently converts to $K_2CO_3 \cdot H_2O$ by absorbing carbon dioxide from the air. Thermal treatment accelerates this process (see below).

In order to obtain detailed information about the thermal stability and possible phase transformations of $K_{2-x}Fe_4O_{7-x}(OH)_x$, a thermogravimetric (TG) analysis coupled to mass-spectrometry (MS) was performed between room temperature and 1000 °C. In addition, annealing experiments in air were carried out over a period of several days in the temperature range of 100 °C to 1000 °C, and temperature-dependent powder X-ray diffraction data, also in air, were recorded between 200 °C to 625 °C in steps of 25 °C. Above approximately 625 °C, the fused silica capillaries broke as they react with the segregated reactive potassium species.

TG under constant flow of synthetic air or argon shows an integral mass loss of 1.5 % in the entire temperature range up to 1000 °C (Figure S8, Supporting Information). The first significant step of the decomposition starts already below 200 °C and is linked with a pronounced peak for $m/z = 18$ in the MS indicating the evaporation of water. The water loss ends at about 400 °C. Between about 400 °C and 550 °C the sample mass remained constant under synthetic air. After this steady state, two minor steps of mass loss are recorded, associated with a steady increase in the MS signal for $m/z = 18$. It should be noted, that the thermal behavior of $K_{2-x}Fe_4O_{7-x}(OH)_x$ is markedly different from that of "$K_2Fe_4O_7$",[9] where neither DTA nor TG signals were found upon heating up to 800 °C.

The temperature-dependent PXRD of $K_{2-x}Fe_4O_{7-x}(OH)_x$ (Figure 9) shows two distinct regimes. In the first stage up to approximately 400 °C, the 2θ values decrease for all reflections, corresponding to a normal thermal expansion. At 400 °C, the unit cell seems to shrink suddenly, especially along the c axis (see below). This is followed by a gradual increase of the lattice parameters and a loss of scattering intensity up to 625 °C. The intermediate reduction of the unit cell volume corresponds to the temperature range of constant mass observed in the TGA.

Single-crystals of $K_{2-x}Fe_4O_{7-x}(OH)_x$ annealed at 350 °C in air showed a superstructure with $a' = 892.03(6)$ pm $\approx \sqrt{3}a$ and $c' =$

Figure 8. Potassium carbonate (bright) covering $K_{2-x}Fe_4O_{7-x}(OH)_x$ crystals (shiny) that are embedded in resin (dark).
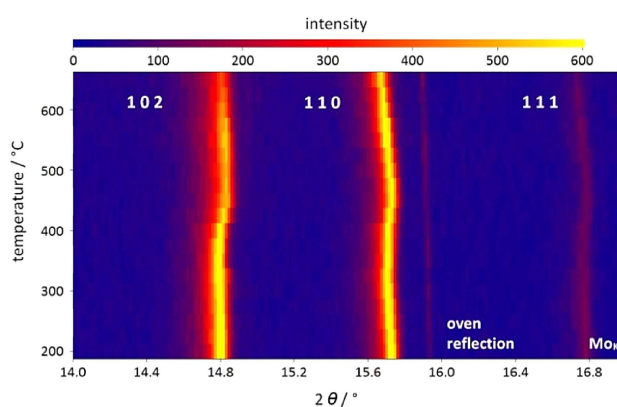

Figure 9. Section of the temperature-dependent PXRD of $K_{2-x}Fe_4O_{7-x}(OH)_x$ in the range of 200 to 650 °C with a heating rate of 1 K/min between the measurements.

2077.6(2) pm ≈ 3c (Figure S9, S10 and Table S5, Supporting Information). The structure, refined in space group $R3$ as inversion twin, shows a partial ordering of potassium ions and vacancies with three differently ordered layers per unit cell. The overall potassium content and the oxoferrate network remain unchanged (Table S6, Supporting Information). The volume of the unit cell with respect to the number of formula unit is only 0.8% smaller than the volume of the original cell and mainly caused by the shrinkage of the c lattice parameter (Table S1 and S5, Supporting Information).

The diffraction pattern of a $K_{2-x}Fe_4O_{7-x}(OH)_x$ single-crystal, that was heated to 500 °C in air with the comparatively high heating rate of 1 K/min and then quenched, showed additional weak reflections that indicate a doubling of all three lattice parameters. The crystal structure of this heated crystal was refined in the space group $P\bar{3}1c$ (Figure S11, S12 and Table S5, Supporting Information). The oxoferrate framework is virtually unchanged again (Table S6, Supporting Information) and the total amount of potassium ($x = 0.32(1)$) is only slightly lower with respect to the pristine sample. In many experiments however, there is a clear trend towards ordering of the potassium atoms in accordance with the hypothetical model for $x = 0.5$ (see above, Figure 4).

Single-crystals of $K_{2-x}Fe_4O_{7-x}(OH)_x$ annealed for three days at 500 °C in air showed another set of weak additional reflections (Figure S13, Supporting Information). These reflections point towards the unit cells of rhombohedral ($R\bar{3}m$) β''-aluminate-type[26,27] or hexagonal ($P6_3/mmc$) β-aluminate-type phases,[30,31] which are both structural variants of $K_{1+x}Fe_{11}O_{17}$. Because of severe stacking faults that emerged in the course of the structural transformation, the periodicity along [001] was not well defined in the annealed crystals and state-of-the-art structure determinations were not possible for these samples.

As the heating rates of the mentioned experiments are very different, their results also reflect the kinetics of the transformation of $K_{2-x}Fe_4O_{7-x}(OH)_x$ into $K_{1+x}Fe_{11}O_{17}$. To simulate an enduring heat stress and to study the thermal stability in air over a long period of time, as it is common for ionic conductors, $K_{2-x}Fe_4O_{7-x}(OH)_x$ samples were annealed for 10 days at various temperatures and then analyzed with PXRD (Figure 14). First weak reflections of $K_{1+x}Fe_{11}O_{17}$ appear for the sample that was annealed at 650 °C (Figure S14, Supporting Information). For the sample annealed at 750 °C the complete conversion of $K_{2-x}Fe_4O_{7-x}(OH)_x$ into $K_{1+x}Fe_{11}O_{17}$ was observed. The β-/β''-aluminate-type phase is stable up to 900 °C. The sample annealed at 900 °C showed traces of maghemite, γ-Fe₂O₃ (Figure S15, Supporting Information). The sample annealed at 950 °C consisted of hematite, α-Fe₂O₃, and traces of γ-Fe₂O₃ (Figure S15, Supporting Information). The latter seems to be an intermediate in the chemical decomposition of $K_{1+x}Fe_{11}O_{17}$, because it was not detected in the sample annealed at 1000 °C (Figure S16, Supporting Information).

The hydrolysis of $K_{2-x}Fe_4O_{7-x}(OH)_x$ to $K_{1+x}Fe_{11}O_{17}$ and the temperature-driven decomposition eventually to Fe_2O_3 can be formalized in two equations:

$$11\,K_{1.5}Fe_4O_7H_{0.5} + 3.5\,H_2O \rightarrow 4\,KFe_{11}O_{17} + 12.5\,KOH \qquad (1)$$

$$2\,KFe_{11}O_{17} \rightarrow 11\,Fe_2O_3 + K_2O \qquad (2)$$

The striking similarity between the crystal structures suggests that the conversion of $K_{2-x}Fe_4O_{7-x}(OH)_x$ into $K_{1+x}Fe_{11}O_{17}$ (equation 1) proceeds by the collapse of alternating pillared layers and the segregation of potassium hydroxide. Although the transformation appears to be topotactic, there must be also migration of iron atoms, as shall be demonstrated in the following.

The structure of $K_{1+x}Fe_{11}O_{17}$ consists of layered spinel type blocks $_\infty^2[Fe_9O_{16}]$ that are separated by the same pillars of vertex-sharing tetrahedra pairs as in $K_{2-x}Fe_4O_{7-x}(OH)_x$. However, the amount of potassium atoms is much lower and the distance between the pillars is wider than in $K_{2-x}Fe_4O_{7-x}(OH)_x$. The latter corresponds again to the hexagonal voids of the kagome nets of octahedra that form the surface layers on both sides of the spinel block (Figure 10). The kagome net has one void per three
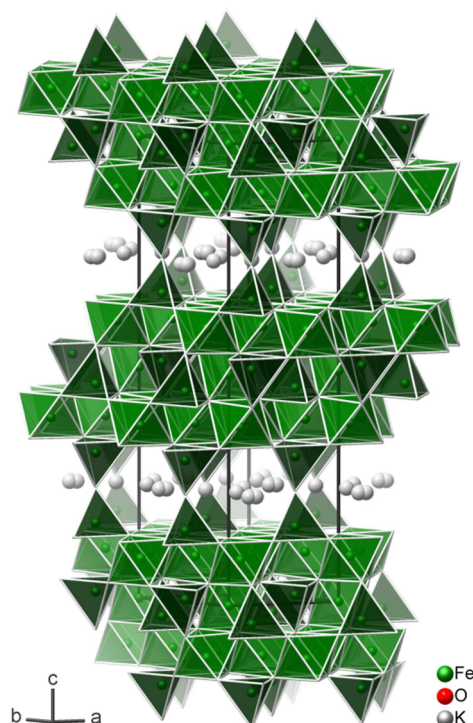

Figure 10. Crystal structure of the hexagonal β-aluminate type $K_{1+x}Fe_{11}O_{17}$.[31]

iron-filled octahedra; the honeycomb net has one void per two iron-filled octahedra (Figure 2). Thus the area of the basal face of the unit cell of $K_{1+x}Fe_{11}O_{17}$ is 4/3 that of $K_{2-x}Fe_4O_{7-x}(OH)_x$. The filled tetrahedral voids in the interior of the spinel layer also cap the hexagonal voids of the kagome layers. The kagome net that forms the opposite surface of the spinel layer is shifted by the vector $v = a/3 + 2b/3$. In Figure 11, the positions of the corresponding tetrahedron's vertex as well as of the filled octahedral void inside the spinel are indicated in red.

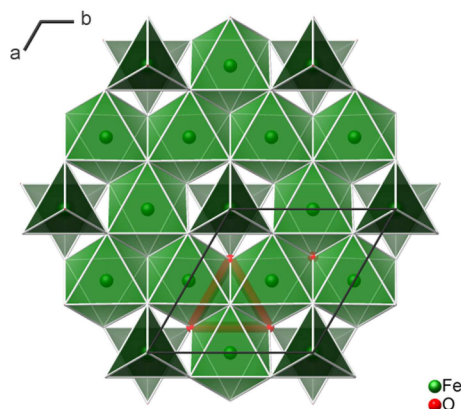The difference between the β- and the β''-type lies in the stacking sequence, which comprises two or three of these

Figure 11. On-top view on a section of the spinel layer in the crystal structure of $K_{1+x}Fe_{11}O_{17}$ (see also Figure 10). The tetrahedra cap the hexagonal voids of the kagome net formed by octahedra in the surface layer. The position of one filled octahedral void inside the spinel layer is indicated by the red triangle. The filled tetrahedral voids are either shown as faded polyhedra or indicated by the red dot, which represents the apical atom of the tetrahedron.

blocks, respectively. The stacking sequence is directed by the conformation of the vertex sharing tetrahedra in the pillars, just as with the two polytypes of $K_{2-x}Fe_4O_{7-x}(OH)_x$ (see above). In the β-type of $K_{1+x}Fe_{11}O_{17}$ they are eclipsed, while in the β″-type they are staggered. Whether the potassium content has an influence on the stacking type, as it was discussed for the alumina compounds, is questionable. It appears more probable that in the underlying case of a topotactic transformation the stacking in the specific $K_{2-x}Fe_4O_{7-x}(OH)_x$ mother crystal, the shift vectors during the breakdown of the columned halls and the additional rearrangement of the iron atoms are decisive.

γ-Fe_2O_3 (maghemite) has a defect-spinel structure (Figure 12) and is thus structurally related to β-/β″-$K_{1+x}Fe_{11}O_{17}$. Actually, the synthesis of β″-$K_{1+x}Fe_{11}O_{17}$ (designated "$K_2Fe_{10}O_{16}$") starting from maghemite has been described in literature.[26]

The mass transport associated with the change in the oxoferrate structure between $K_{2-x}Fe_4O_{7-x}(OH)_x$ to $K_{1+x}Fe_{11}O_{17}$
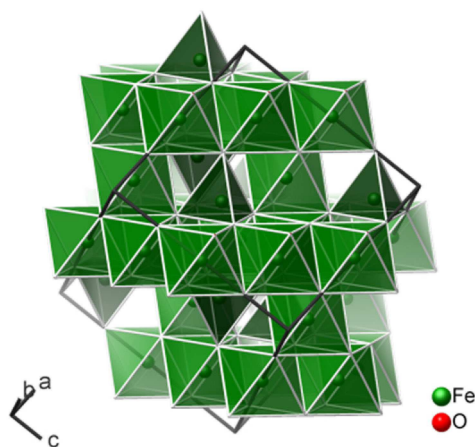

Figure 12. The (defect-)spinel structure of γ−Fe_2O_3 (maghemite) in a projection analogous to the one in Figure 10.

can be balanced by regarding corresponding volumes within the two structures (stoichiometric $K_2Fe_4O_7$ assumed for simplicity):

$K_2Fe_4O_7$: $2 \times 4 \times \{[Fe_2\square O_6]_O \cdot [Fe_2O]_T\}$

$= [Fe_{16}O_{48}]_O \cdot [Fe_{16}O_8]_T$

$= Fe_{32}O_{56}$

$KFe_{11}O_{17}$: $3 \times \{2[Fe_3\square O_8]_O \cdot [Fe_2O]_T \cdot [Fe_2]_T \cdot [Fe]_O\}$

$= [Fe_{18}O_{48}]_O \cdot [Fe_6O_3]_T \cdot [Fe_6]_T \cdot [Fe_3]_O$

$= Fe_{33}O_{51}$

The structured formulas show that no oxygen from the layers is lost; formally the KOH takes the spiro-oxygen atom of the pillars out of the crystal. Of 16 tetrahedrally coordinated iron atoms that form the pillars in $K_{2-x}Fe_4O_{7-x}(OH)_x$, six remain pillars in $K_{1+x}Fe_{11}O_{17}$ (yet change their position), six remain tetrahedrally coordinated inside the spinel layer, three become octahedrally coordinated inside the spinel layer, and two enter the honeycomb layers of octahedra and transform them into kagome nets. Oddly, this consideration creates an additional iron atom in the referenced volume, whose origin cannot be explained. In fact, the structure determination of the β″-type crystal yielded the composition $K_{1.81}Fe_{10.73}O_{17}$, i.e. in our consideration, an oxoferrate sum formula close to $Fe_{32}O_{51}$.[27] Hence, it seems highly probable that additional voids on iron positions exist (as in γ−Fe_2O_3) and the "idealized" sum formula of a crystal obtained by decomposition of $K_{2-x}Fe_4O_{7-x}(OH)_x$ should be $K_2Fe_{10.67}O_{17}$. However, this is based on the assumptions of the oxidation state +III for all iron atoms, no oxygen vacancies, no residuals of the mother structure, and no further collapse to thicker spinel layers. Hence, there are many options for a phase-width.

The consequences of the de-intercalation of KOH for the real structure of the crystals can be seen in Figure 13. The
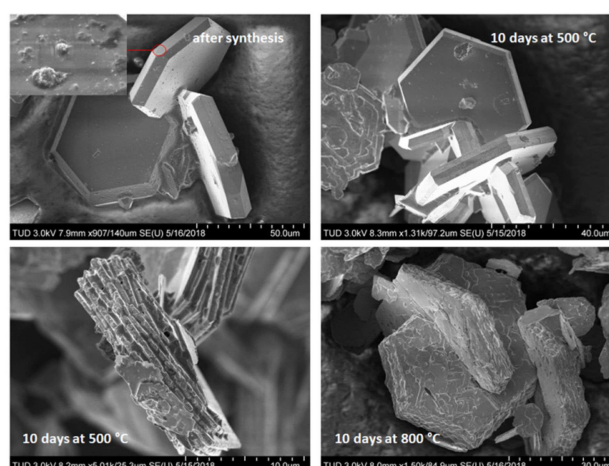

Figure 13. SEM images of samples of $K_{2-x}Fe_4O_{7-x}(OH)_x$ kept for some days at ambient conditions as well as after annealing in air for 10 days at 500 °C and 800 °C.

crystals stored at ambient conditions show small crumbs with irregular shapes on the otherwise smooth surface. EDX measurements on these crumbs indicated potassium and carbon, probably due to the formation of potassium carbonate, as already discussed above. Most of the $K_{2-x}Fe_4O_{7-x}(OH)_x$ crystals annealed at 500 °C are scarcely changed (Figure 13, upper right). Yet, some crystals have split along the crystallographic *c* direction into several platelets. A segregation product is clearly visible between these platelets, probably consisting of potassium carbonate, based on EDX analysis. In SCXRD as well as in PXRD (Figure 14) measurements of nearly all annealed
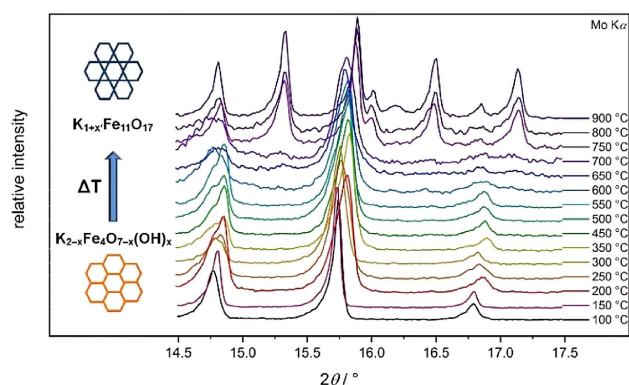

Figure 14. Sections of the PXRD pattern of samples of $K_{2-x}Fe_4O_{7-x}(OH)_x$ that were annealed for 10 days at the given temperature in air and then analyzed at room temperature.

samples, a broadening of the reflections and a higher mosaicity were observed, even for crystals with smooth surfaces. This corresponds to the water loss evidenced by TG/MS. Crystals treated at 800 °C, generally show a rough and flaky surface. Although the crystal shape is mainly unchanged, these samples are completely converted to $K_{1+x}Fe_{11}O_{17}$, as confirmed by P-XRD.

3. Conclusions

Phase pure potassium oxo-hydroxoyferrate $K_{2-x}Fe_4O_{7-x}(OH)_x$ ($x \approx 0.3$) is obtained by reaction of $Fe(NO_3)_3 \cdot 9H_2O$ with KOH under hydroflux conditions at about 200 °C in a quantitative yield. The crystal structure of $K_{2-x}Fe_4O_{7-x}(OH)_x$ comprises edge-sharing $[FeO_6]$ octahedra in a honeycomb net $_\infty^2[Fe_2O_6]$. Adjacent honeycomb nets are connected by pairs of vertex-sharing $[FeO_4]$ tetrahedra, the large voids between the honeycomb layers – which can be viewed as columnar halls – host the potassium atoms. The sub-stoichiometric potassium content is compensated by hydroxide groups, however hydrogen positions could not be located from X-ray or neutron scattering data. The trigonal ($P\bar{3}1m$) and the hexagonal ($P6_3/mcm$) polytypes of $K_{2-x}Fe_4O_{7-x}(OH)_x$ show oriented intergrowth. Above 2 K $K_{2-x}Fe_4O_{7-x}(OH)_x$ is an antiferromagnet and decomposes before the Néel temperature is reached. The magnetic structure was determined by neutron powder diffraction. $K_2CO_3 \cdot H_2O$ forms gradually on the surface of $K_{2-x}Fe_4O_{7-x}(OH)_x$ crystals

stored under ambient conditions due to partial hydrolysis. At higher temperatures, several structural changes set in. At about 350 °C, the potassium ions start to order into a superstructure. Upon further heating to about 750 °C, $K_{2-x}Fe_4O_{7-x}(OH)_x$ transforms topotactically into $K_{1+x}Fe_{11}O_{17}$ with the rhombohedral β'' or the hexagonal β-aluminate-type structure. The final decomposition starts at 900 °C with formation of γ-Fe_2O_3, which then converts into the stable polymorph α-Fe_2O_3.

Experimental Section

Synthesis

The potassium ferrate $K_{2-x}Fe_4O_{7-x}(OH)_x$ ($x \approx 0.3$) was synthesized in potassium hydroxide hydroflux reactions. Syntheses were carried out in PTFE-lined 23 mL Parr type 4749 A autoclaves to prevent loss of water. In a typical synthesis the hydroflux consisted of 6.5 g potassium hydroxide (85 %, VWR Chemicals) and 2 mL deionized water (molar ratio 1.0 : 1.2). To this solid mixture 1.212 g (3 mmol) of $Fe(NO_3)_3 \cdot 9H_2O$ (≥ 98 %, Alfa Aesar) were added. An air-filled headspace of about 15 mL remained. The autoclave was heated to 200 °C with 2 K/min and held for 10 h at this temperature before cooling down to room temperature at the rate of 0.5 K/min. The red hexagonal crystals were isolated by washing with deionized water.

Powder X-ray Diffraction

Phase identification and purity examinations were performed by powder X-ray diffraction (PXRD) at room temperature on an STADI P diffractometer (Stoe & Cie) equipped with a Dectris Mythen 1 K detector using Ge monochromated Mo-$K\alpha_1$ radiation ($\lambda = 70.932$ pm). The same diffractometer was used with a capillary oven setup (graphite heating element) between 25 °C and 625 °C with a heating rate of 1 K/min and with nitrogen as inert gas.

Neutron Diffraction

The characterization of the magnetic order was carried out on the SPODI high-resolution powder diffractometer at the research reactor Heinz Maier-Leibnitz in Munich (FRM II) using neutrons with the wave length $\lambda = 154.81$ pm. The detector consists of 80 spatially resolved ^{3}He counter tubes (active measuring height: 300 mm), each of these counter tubes having an angular range of 2°. The data acquisition of a 160° measurement typically occurs in 40 steps ($\Delta(2\theta) = 0.05$°).[32]

SEM and EDX Analysis

Scanning electron microscopy (SEM) was performed using a SU8020 (Hitachi) with a triple detector system for secondary and low-energy backscattered electrons ($U_a = 3$ kV). The composition of selected single crystals was determined by semi-quantitative energy dispersive X-ray analysis ($U_a = 10$ kV) using a Silicon Drift Detector (SDD) X-Max^N (Oxford).

IR-Spectroscopy

IR spectra were recorded using a Bruker Vertex 70 FT-IR spectrometer. The device was operated in the ATR mode

(diamond), working with a measuring range of 4000 to 250 cm^{-1}. The software used to evaluate the spectra was Opus 6.5.[33]

TGA

K$_{2-x}$Fe$_4$O$_{7-x}$(OH)$_x$ samples were heated under a dynamic flow of synthetic (without CO$_2$) air or argon in a STA 409 C/CD (Netzsch). The samples were heated to 1000 °C at rates of 0.5 to 5 °C/min.

ICP-OES

The ICP-OES measurements were carried out on an Optima 7000 DV optical emission spectrometer (Perkin-Elmer). The device can process the wavelength range of 160–900 nm with a high-resolution echelle optics (30° CaF$_2$ prism) on an SCD detector (resolution < 7 pm).

Carrier Gas Hot Extraction

The hydrogen and oxygen content of K$_{2-x}$Fe$_4$O$_{7-x}$(OH)$_x$ was analyzed by using a TCH600 carrier gas hot extraction system from Leco. To exclude side products like potassium carbonate on the surface of the measured sample, the carbon content was also determined with a CS744 from Leco.

Magnetization Measurements and Electrical Resistance

The low temperature magnetic properties were analyzed on a Cryogen Free Measurement System (CFMS), Cryogenic Ltd. The magnetization data were recorded using a Vibrating Sample Magnetometer (VSM, 21 Hz, 2 to 300 K). The electrical resistivity of a single-crystal between 2 K and 300 K (1 K/min as heating rate) was measured using gold contacts and carbon conductive composite 7105 (DuPont). The high temperature magnetic properties were analyzed on the SQUID magnetometer MPMS3 with oven from Quantum Design in VSM mode in a temperature range of 300 K to 950 K with a heating rate of 10 K/min.

Crystal Structure Determination

Intensity data were collected at 100 K with a four-circle diffractometer Kappa Apex2 (Bruker) equipped with a CCD-detector using graphite-monochromated Mo-$K\alpha$ radiation ($\lambda = 71.073$ pm). Data were corrected for Lorentz and polarization factors,[34] and multi-scan absorption correction was applied.[35] The structure was solved with Direct Methods using ShelXT.[36] Structure refinement against F_o^2 with ShelXL[37] included anisotropic displacement parameters for all atoms. Crystallographic data have been deposited with Fachinformationszentrum Karlsruhe, D-76344 Eggenstein-Leopold-shafen (Germany) and can be obtained on quoting the depository numbers CSD-1875190 (pristine sample), CSD-1875193 and CSD-1875189 (magnetic structure at 4 K and 300 K, respectively) and CSD-1875192 and CSD-1875191 (samples annealed at 350 °C and 500 °C, respectively).

Mößbauer Spectroscopy

A ^{57}Co/Rh source was used for the ^{57}Fe Mößbauer spectroscopic measurements. The sample was placed in a PMMA container and the measurement was run in the usual transmission geometry at 6 K. Fitting of the spectrum was performed with the Normos-90 program system.[38]

Conflict of Interest

The authors declare no conflict of interest.

[1] G. Tan, X. Chen, *J. Magn. Magn. Mater.* **2013**, *327*, 87–90.
[2] P. L. Knöchel, P. J. Keenan, C. Loho, C. Reitz, R. Witte, K. S. Knight, A. J. Wright, H. Hahn, P. R. Slater, O. Clemens, *J. Mater. Chem. A* **2016**, *4*, 3415–3430.
[3] C. Xia, Y. Jia, M. Tao, Q. Zhang, *Phys. Lett.* **2013**, *377*, 1943–1947.
[4] S. S. Shinde, R. A. Bansode, C. H. Bhosale, K. Y. Rajpure, *J. Semicond.* **2011**, *32*, 013001.
[5] R. C. Pullar, *Prog. Mater. Sci.* **2012**, *57*, 1191–1334.
[6] D. M. Sherman, *Phys. Chem. Miner.* **1985**, *12*, 161–175.
[7] C. Allègre, G. Manhès, É. Lewin, *Earth Planet. Sci. Lett.* **2001**, *185*, 49–69.
[8] H. Yuan, H. Li, T. Zhang, C. Zhang, S. Feng, *Potassium Ferrite and Preparation Method Thereof*, **2017**, CN 201510245772.
[9] H. Yuan, H. Li, T. Zhang, G. Li, T. He, F. Du, S. Feng, *J. Mater. Chem. A* **2018**, 8413–8418.
[10] M. Gogolin, M. M. Murshed, T. M. Gesing, 25th Annual Conference of the German Crystallographic, *Z. Kristallogr.* **2017**, 119.
[11] D. E. Bugaris, M. D. Smith, H.-C. zur Loye, *Inorg. Chem.* **2013**, *52*, 3836–3844.
[12] W. M. Chance, D. E. Bugaris, A. S. Sefat, H.-C. zur Loye, *Inorg. Chem.* **2013**, *52*, 11723–11733.
[13] G. Chen, X. Wang, J. Wang, H. Du, Y. Zhang, S.-L. Zheng, Y. Zhang, *Int. J. Miner. Process.* **2014**, *131*, 58–68.
[14] T. Ferreira, G. Morrison, W. M. Chance, S. Calder, M. D. Smith, H.-C. zur Loye, *Chem. Mater.* **2017**, *29*, 2689–2693.
[15] T. Matsuzaki, K. Hagiya, A. Shatskiy, T. Katsura, M. Matsui, *J. Mineral. Petrol. Sci.* **2010**, *105*, 303–308.
[16] H. Yang, J. Konzett, C. T. Prewitt, *Am. Mineral.* **2001**, 1483–1488.
[17] S. Okamato, S. I. Okamato, T. Ito, *Acta Crystallogr.* **1973**, 832–838.
[18] M. Posfai, M. Sundberg, *Am. Mineral.* **1998**, *83*, 365–372.
[19] S. Ďurovič, P. Krishna, D. Pandey, *Int. Tables Crystallogr. Vol C* **2006**, 752–773.
[20] B. B. Zvyagin, *Comput. Math. Appl.* **1988**, *16*, 569–591.
[21] R. A. Nyquist, R. O. Kagel, *Infrared Spectra of Inorganic Compounds*, Academic Press Inc., New York and London, **1971**.
[22] H. D. Lutz, in *Structure and Bonding*, Springer Berlin Heidelberg, Berlin, Heidelberg, **1995**, pp. 85–103.
[23] M. Abaker, A. Umar, S. Baskoutas, G. N. Dar, S. A. Zaidi, S. A. Al-Sayari, A. Al-Hajry, S. H. Kim, S. W. Hwang, *J. Phys.* **2011**, *44*, 425401.
[24] E. K. Abdel-Khalek, H. M. Mohamed, *Hyperfine Interact.* **2013**, *222*, 57–67.
[25] F. Menil, *J. Phys. Chem. Solids* **1985**, *46*, 763–789.
[26] S. Nariki, S. Ito, N. Yoneda, *Am. Ceram. Soc. Bull.* **1987**, 1250.

[27] N. Z. Ali, J. Nuss, D. Sheptyakov, M. Jansen, *J. Solid State Chem.* **2010**, *183*, 752–759. (ICSD: 174323)

[28] A. L. Hector, J. A. Hutchings, R. L. Needs, M. F. Thomas, M. T. Weller, *J. Mater. Chem.* **2001**, *11*, 527–532.

[29] L.-S. Xie, G.-X. Jin, L. He, G. E. W. Bauer, J. Barker, K. Xia, *Phys. Rev. B* **2017**, *95*, 014423.

[30] S. Ito, H. Kurosawa, K. Akashi, Y. Michiue, M. Watanabe, *Solid State Ionics* **1996**, *86*, 745–750.

[31] J. P. Boilot, P. Colomban, G. Collin, R. Comes, *Solid State Ionics* **1980**, *1*, 69–76.

[32] M. Hoelzel, A. Senyshyn, R. Gilles, H. Boysen, H. Fuess, *Neutron News* **2007**, *18*, 23–26.

[33] *Opus 6.5*, Bruker Optik, **2007**.

[34] *APEX2*, Bruker AXS Inc., Madison, Wisconsin, USA, **2014**.

[35] G. M. Sheldrick, *Sadabs: Area-Detector Absorption Correction*, Bruker AXS Inc., Madison, Wisconsin, USA, **2014**.

[36] G. M. Sheldrick, *ShelXT*, Universität Göttingen, Germany, **2014**.

[37] G. M. Sheldrick, *Acta Crystallogr. Sect. A* **2008**, 112–122.

[38] R. A. Brand, *Normos*, Normos Mössbauer Fitting Program, University of Duisburg, Duisburg (Germany), **2002**.